Proceedings of the 21st ICSMGE, Vienna, Austria, 14 – 19 June 2026. Pistrol, Adam & Schweiger (eds.)
Published by: ÖGG, Austrian Society for Geomechanics, Salzburg, Austria, ISBN 978-3-9503898-4-5
https://doi.org/10.53243/ICSMGE2026-393

Evolution of the force chain network beneath a strip foundation

Barbara Świtała, Danuta Leśniewska, Justyna Sławińska-Budzich, Muzafar Ali Kalwar
Institute of Hydro-Engineering, Polish Academy of Sciences, Poland, b.switala@ibwpan.gda.pl

ABSTRACT: Accurately assessing the bearing capacity of shallow foundations is essential for their efficient design. Strip foundations, a specific type of shallow foundations, are designed to support load-bearing walls, allowing the assumption of plane strain conditions in experimental and numerical analyses. The stress state beneath a foundation is a key factor influencing its bearing capacity. This study employs photoelastic methods to visualize the stress field beneath a strip foundation under plane strain conditions. Transparent PDMS (Polydimethylsiloxane) grains, manufactured and tested in-house, are used to create the experimental sample. The experimental results serve as a base for calibration and verification of the numerical simulations based on the discrete element method (DEM). A well-calibrated numerical model acts as a virtual laboratory, enabling detailed sensitivity analyses to explore the effects of varying material parameters or loading scenarios on the force network structure and foundation settlement behavior. Additionally, novel image correlation techniques are employed to extract strain fields from image sequences. This information, combined with force chain distributions, offers valuable insights for refining and verifying existing bearing capacity models.

KEYWORDS: Photoelasticity, strip foundation, Discrete Element Methods, virtual laboratory, sensitivity analysis.

1 INTRODUCTION

The stress field in soil under foundation loading cannot be directly visualized through conventional experimental methods. Soil bearing capacity is measurable, structural influence zones are identifiable through modeling, and soil strength parameters are derived from laboratory procedures. Tomographic imaging provides insight into the sample's internal structure. However, the transmission pattern of forces, along with their magnitude, remains inaccessible using these techniques.

Photoelastic methods enable stress visualization in loaded transparent materials, which exhibit birefringence, visible under polarized light. This method, initially discovered in solid materials, has been successfully applied to study stress field and force transmission pattern in transparent granular materials (Wakabayashi, 1960, Dantu, 1957, Drescher & De Jong, 1957, Majmudar & Behringer, 2005). Recently, photoelastic methods have gained significant attention due to the advancements in image correlation analyses and discrete element methods (DEM) (Cundall & Strack 1979), which offer new possibilities. The load transmission paths in the granular system are called “force chains”. They can be defined as a finite linear structure of contacting grains, transmitting boundary loads through a granular material to the point where it reaches some minimum value (Świtała et al. 2024).

In the present study, a photoelastic experiment is conducted to visualize the force chain network beneath a loaded strip foundation. Based on this experiment, a digital model is developed using DEM and calibrated to closely reflect the material's behavior. This model enables extensive sensitivity analyses to examine the influence of various material parameters and test conditions on the results, specifically, the structure of the force chain network and foundation settlements. The analysis will encompass the sensitivity of the changes in friction coefficient and rolling friction coefficient.

2 EXPERIMENT

2.1 *Materials and methods*

The experimental setup consisted of a transparent box, shown in Figure 1, filled with transparent polydimethylsiloxane (PDMS) granules, which were manufactured and tested in-house, up to a height of 17.6 cm. The box thickness was 2.0 cm. To maximize optical transparency, the photoelastic particles were immersed in a liquid with a matching refractive index. Since the density of PDMS is slightly lower than that of the immersion liquid, the granules were loaded with heavier material, such as steel beads, to ensure proper immersion. Additionally, a layer of steel beads served as the surface surcharge in a bearing capacity test. The foundation model was a rectangular prism made of polished stainless steel (Young’s modulus of about 200 GPa) and was placed centrally on the layer of PDMS granules. Then, the loading system was installed and placed on the top of the foundation. The initial mass of the entire setup was 600g, which corresponded to the pressure of 5.9 kPa. Settlements observed under this reference load served as a baseline for evaluating those resulting from subsequent load increments.

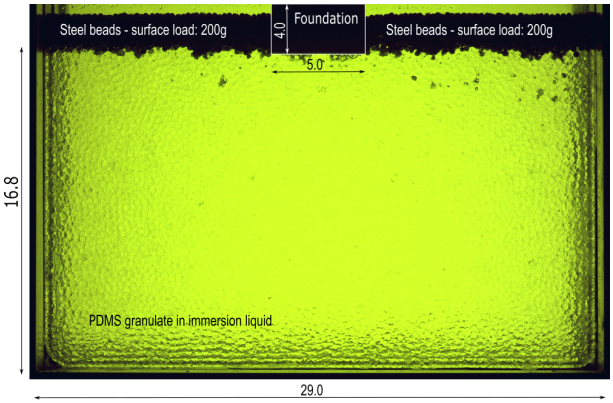

Figure 1. Geometry of the box test and initial conditions.

Incremental loading was achieved by pouring lead shot of appropriate mass into a bin positioned above the foundation, from which the load was transmitted to the foundation via a rigid vertical rod. The loading scheme consisted of 65 steps. From 5.9 kPa to 14.7 kPa, the load was increased in 0.981 kPa increments, followed by 1.962 kPa increments until a total of 107.9 kPa was reached. Foundation failure was then induced by a rapid surcharge, increasing the load to 142.25 kPa, which was achieved by placing the set of weights on the top of the bin.

2.2 *Results*

Significant information was extracted from the images captured at each load increment, under both normal and polarized light. First, a stepwise settlement pattern was identified and analyzed. Figure 2 presents the settlement curve as a function of the applied load. The settlement level increased approximately linearly with successive load increments, up to 107.9 kPa, which is the maximum load achievable with the employed loading system. Subsequently, additional, much larger weights

were applied, which induced rapid foundation failure. As a result, a sudden loss of bearing capacity in the granular system led to a reported settlement of nearly 20 mm.

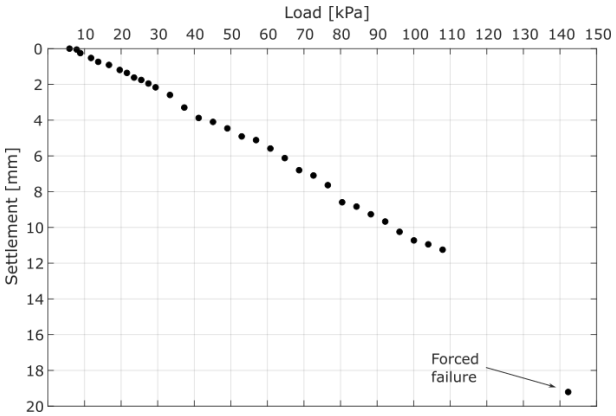

Figure 2. Foundation settlement under applied load.

Throughout the loading program, a complex network of force chains developed, revealing the transmission paths within the granular system and distinctly highlighting a bulb-shaped zone strongly influenced by the loaded foundation. The force chain network, photographed under polarized light and corresponding to a load of 107.9 kPa, is presented in Figure 3.

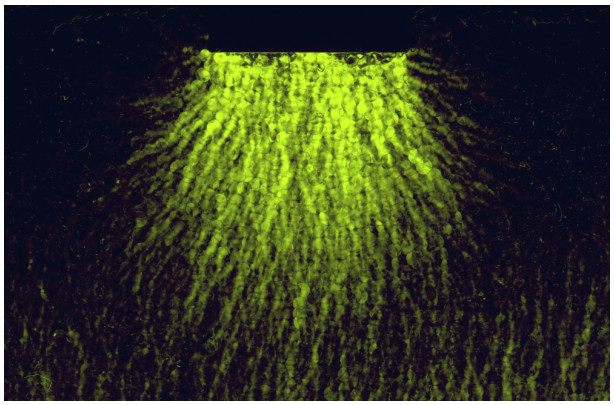

Figure 3. Force chain network in a polarized light.

The brightest colours illuminate the force chains connecting the most heavily loaded grains. Directly beneath the centre of the foundation, these chains predominantly follow the loading direction. However, deeper into the granular medium, and near the foundation corners, their orientation progressively shifts outward, diverging toward the sides.

2.3 *Image analysis*

The loaded sample was photographed at each load increment under normal lighting conditions. Although the sample exhibited relatively good transparency, it was still possible to capture the grain contours. This information is essential for conducting Digital Image Correlation (DIC) using DaVis software. The analysis revealed the maximum shear strain contours in response to the applied load. The resulting image, corresponding to a pressure of 107.9 kPa exerted on the foundation, is presented in Figure 4.

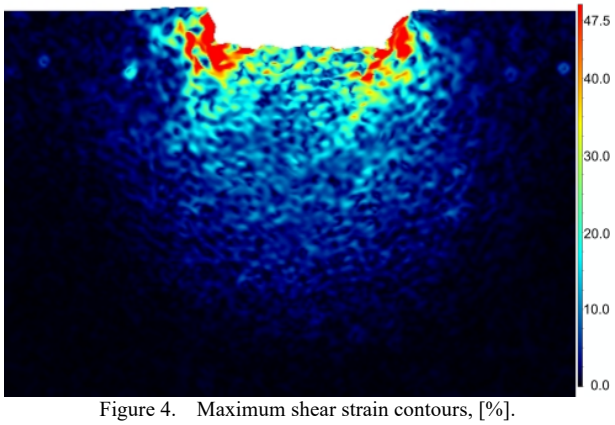

Figure 4. Maximum shear strain contours, [%].

3 NUMERICAL MODELLING

3.1 *Initial conditions*

The experiment described in the previous section was numerically simulated using the Discrete Element Method (DEM). Calculations were conducted with LIGGGHTS software (Kloss et al. 2012), employing the Hertz-Mindlin contact model to characterize inter-particle interactions. In the sensitivity analyses investigating the influence of rolling friction, the Constant Directional Torque (CDT) model was additionally incorporated.

The model geometry corresponded to the experimental setup. A total of 27,746 PDMS spherical grains were simulated, resulting in a porosity of approximately 42%. Initially, grains were poured into the box until a sample height of 16.8 cm was reached. Subsequently, the foundation was placed on top of the granular assembly. Steel beads were then poured on both sides of the foundation, simulating a surface surcharge mass of 200 g (about 0.8 kPa) per side. The PDMS parameters used in the numerical simulations are listed in Table 1. This set of parameters provides an accurate fit between the numerical and experimental results.

Table 1. PDMS parameters used in the numerical model.

Parameter	Symbol	Value	Unit
Young's modulus	E	21.97	MPa
Poisson's ratio	ν	0.495	-
Density	ρ	970.0	kg/m^3
Friction coeff. PDMS-PDMS	μ_s	0.59	-
Friction coeff. PDMS-glass	μ_{wall}	0.5	-
Restitution coeff. PDMS	e_r	0.6	-
Restitution coeff. PDMS-glass	$e_{r,walls}$	0.7	-

3.2 *Results*

In the numerical simulations, small loading steps of 1.962 kPa are applied beyond 107.9 kPa (11 kg), until the bearing capacity of the granular assembly is exceeded, resulting in rapid settlement accumulation. Prior to this point, the settlement-load curve follows an approximately linear trajectory. Figure 5 illustrates the settlement curve as a function of the applied load, comparing the experimental outcomes with the numerical predictions.

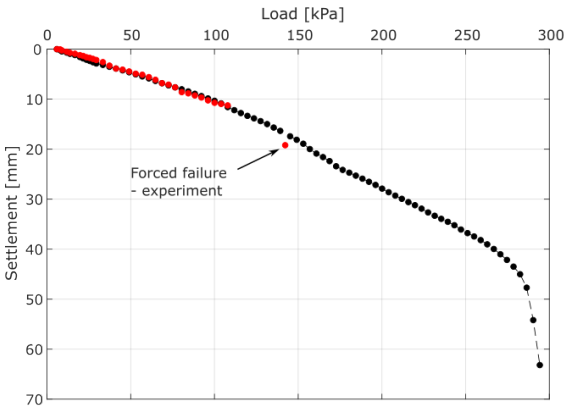

Figure 5. Foundation settlements from the experiment and numerical analyses, plotted as a function of the applied load.

Similarly to the experiment, the numerical simulations showed that a complex force chain network developed incrementally in response to successive load increments. Since the well-calibrated numerical model can serve as a virtual laboratory for predicting material behavior under various loading conditions, it is possible to analyze the development of the force chain network at higher load increments than those applied in the experiment. Furthermore, the model allows for a deeper investigation into the failure mechanisms and the associated transformation of the sample's microstructure. The force chain network, which is a result of numerical calculations, corresponding to the load of 266.8 kPa (prior to failure), and 274.7 kPa (after failure), is presented in Figure 6.

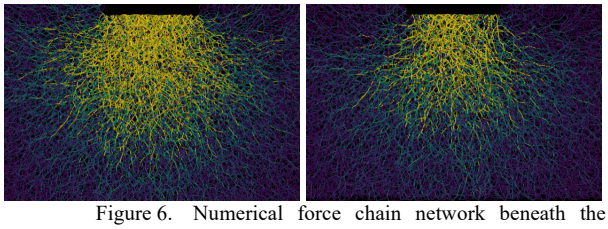

Figure 6. Numerical force chain network beneath the foundation, prior to failure (left), after failure (right).

The force chain network derived from the simulations reveals finer structural detail than that observed experimentally. Even very weak chains are visible, allowing for the identification of branching patterns and the inclination of chains relative to the loading direction. Prior to failure, the force chain structure is highly developed and complex. Load transmission is generally directed vertically downward; however, numerous chains extend horizontally. This suggests that grains are being displaced from beneath the foundation toward the sides and upward, resulting in the uplift of surface grains. After failure, the force chain network appears darker, indicating reduced force intensity. Several chains are broken, particularly near the corners of the foundation. Therefore, the force transmission pattern is disturbed, and granular assembly cannot sustain additional loading without undergoing significant displacements.

4 SENSITIVITY ANALYSES

The application of DEM modeling facilitates the investigation of how different material and model parameters affect simulation outcomes. In this study, particular attention was given to examining the influence of the friction coefficient and rolling resistance between PDMS particles on foundation settlement patterns.

4.1 *Friction coefficient*

The friction coefficient between PDMS particles governs their resistance to sliding at contact interfaces. As a result, it serves as a critical parameter in discrete element analyses and is expected to exert a substantial influence on the simulation outcomes.

In this study, four values of the friction coefficient were examined: the reference value of 0.59, along with additional values of 0.50, 0.40, and 0.30. The influence of this parameter on the course of the settlement–loading curve is illustrated in Figure 7.

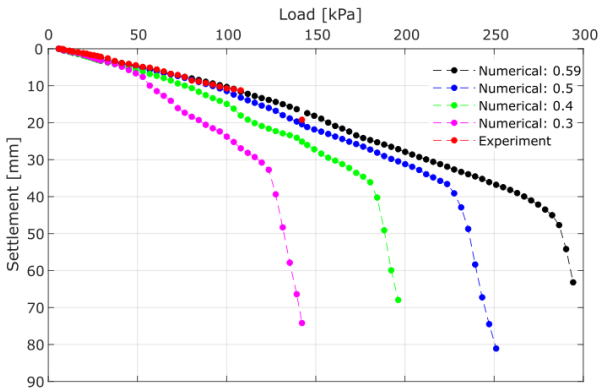

Figure 7. Influence of friction coefficient on the settlement-loading curve.

From this figure, we can observe that decreasing friction coefficient leads to more pronounced settlements under the same load, compared to the reference case where the coefficient was 0.59. Interestingly, although failure occurs at lower pressure values for reduced friction coefficients, the settlement level at which the curve shifts from a gentle to a nearly vertical inclination remains similar across all cases. Therefore, we can conclude that the level of settlement governs the onset of failure, which is naturally influenced by the pressure exerted on the foundation. For higher friction coefficients, greater pressure is required to induce settlements corresponding to the failure state than for lower values of this parameter.

The reason behind this is that grains with lower friction coefficients can be displaced more easily under lower pressure, as less force is required to initiate movement. Consequently, the structure formed by these grains is less stable compared to the one formed by grains with higher friction coefficients.

Apart from variations in the load–settlement curve, differences in the friction coefficient also influence the structure of the force chain network, as shown in Figure 8. All subfigures depict the network corresponding to a similar level of foundation settlement, approximately 40 mm.

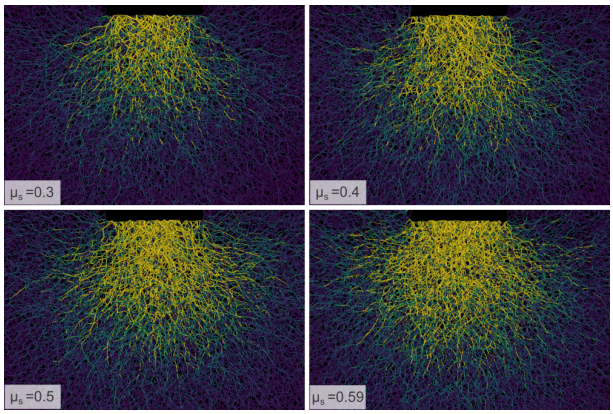

Figure 8. Force chain network beneath the foundation – results for different friction coefficients.

The force chain network that formed beneath the foundation in simulations with lower friction coefficients appears significantly less developed. As the friction coefficient increases, the network becomes more complex and exhibits higher contact force magnitudes, indicated by brighter colors.

4.2 *Rolling friction coefficient*

Another material parameter explored in this study is the rolling friction coefficient. In LIGGGHTS software, rolling friction can be modeled using the Constant Directional Torque (CDT) approach, which applies a torque at the contact interface between particles, counteracting their relative rotational motion. In the reference scenario, rolling friction is not considered. However, in the sensitivity analysis, three distinct values are examined: 0.1, 0.15, and 0.2.

The influence of the rolling friction coefficient on the settlement-loading curve is illustrated in Figure 9. For this analysis, the range of applied loads has been extended to 400 kPa. Within this range, failure, indicated by a rapid accumulation of settlements, does not occur when the rolling friction coefficient is nonzero.

Moreover, the shape of the loading-settlement curve does not vary significantly across different values of the considered parameter. Furthermore, the results of the analyses align with the experimental results within the corresponding load range; however, the reference case (with a rolling friction coefficient of zero) appears to match the experimental data most accurately. The presence of rolling resistance makes it more difficult for grains to rearrange, thereby adding an additional stabilizing effect to the assembly. This may explain why failure does not occur within the considered load range.

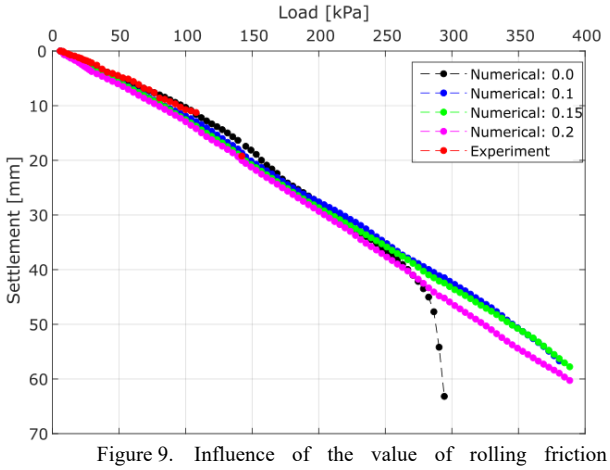

Figure 9. Influence of the value of rolling friction coefficient on the settlement-loading curve.

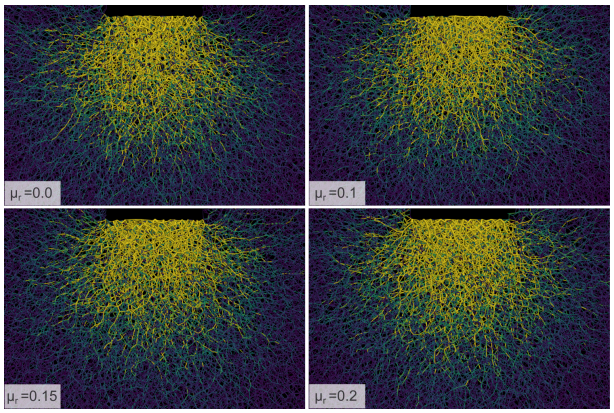

Figure 10. Force chain network beneath the foundation – results for different rolling friction coefficients

The force chain network corresponding to a load of 266.8 kPa (just prior to failure in the reference case) is presented in Figure 10 for all considered rolling resistance scenarios. The structure and shape of the networks do not differ significantly. Although individual chains follow different paths and vary in length, the overall pattern remains similar. For the case with a rolling friction coefficient of 0.2, the network appears slightly more developed and extends deeper beneath the foundation.

5 CONCLUSIONS

This paper presents a brief description of the photoelastic experiment, which provides a basis for calibrating the DEM model. Once properly calibrated, such a model can serve as a virtual laboratory for testing various material parameters and initial conditions, and for analyzing the resulting behavior.

We conducted a sensitivity analysis on the effects of changes in the friction coefficient and rolling friction coefficient. The results revealed that accurate selection of the friction coefficient is critically important and has a significant influence on the shape of the load–settlement curve. When rolling resistance is considered, the sample appears to gain additional stability, and failure is not triggered within the examined load range.

The visualization of the force chain network, combined with the availability of modern tools that enable its reproduction and detailed analysis, such as DEM and DIC, opens new possibilities for investigating the behavior of granular materials under various loading scenarios. Observations made at the micro and meso scales play a crucial role in interpreting the results of macro-scale analyses and in the development of more detailed and accurate models.

Furthermore, in practice, such models, when properly calibrated, may be useful for predicting settlement levels and the bearing capacity of foundations, taking into account, for example, optimization of their shape or variations in soil parameters.

6 ACKNOWLEDGEMENTS

This research was funded by the National Science Centre, Poland, project No. 2020/39/B/ST8/01685. For the purpose of Open Access, the authors has applied a CC-BY public copyright licence to any Author Accepted Manuscript (AAM) version arising from this submission.

7 REFERENCES

Cundall, P. A., and Strack, O. D. 1979. A discrete numerical model for granular assemblies. *Geotechnique*, *29*(1), 47-65.

Dantu, P. 1957. Contribution à l'étude mécanique et géométrique des milieux pulvérulents. *Proc. 4th ICSMFE*, London.

Drescher, A., and De Jong, G. D. J. 1972. Photoelastic verification of a mechanical model for the flow of a granular material. *Journal of the Mechanics and Physics of Solids*, *20*(5), 337-340.

Majmudar, T. S., and Behringer, R. P. 2005. Contact force measurements and stress-induced anisotropy in granular materials. *Nature*, 435(7045), 1079-1082.

Kloss, C., Goniva, C., Hager, A., Amberger, S., and Pirker, S. 2012. Models, algorithms and validation for opensource DEM and CFD–DEM. *Progress in Computational Fluid Dynamics, an International Journal*, 12(2-3), 140-152.

Świtała, B., Leśniewska, D., and Kalwar, M. A. 2024. Micro-mechanisms of force network rearrangement in granular materials. *Computers and Geotechnics*, *174*, 106602.

Wakabayashi, T. 1960. Photoelastic studies of the stress in powder mass. *Soils and Foundations*, 1(2), 12-22.